

Probabilities of polar aligned disks in binary star systems

TED JOHNSON,^{1,2} REBECCA G. MARTIN,^{1,2} STEPHEN LEPP,^{1,2} AND Stephen H. Lubow³

¹*Nevada Center for Astrophysics, University of Nevada, Las Vegas, 4505 South Maryland Parkway, Las Vegas, NV 89154, USA*

²*Department of Physics and Astronomy, University of Nevada, Las Vegas, 4505 South Maryland Parkway, Las Vegas, NV 89154, USA*

³*Space Telescope Science Institute, 3700 San Martin Drive, Baltimore, MD 21218, USA*

ABSTRACT

Inclined circumbinary disks settle to coplanar or Circumbinary gas disks that are misaligned to the binary orbital plane evolve toward either a coplanar or a polar-aligned configurations configuration with respect to the binary host. The preferred alignment can be found analytically in the case limit of a massless disk, however disk-star disk-binary interactions make the general massive disk case much more challenging. We employ the N-body code REBOUND rebound to investigate the dynamics of these 3-body systems and use Monte Carlo methods to quantify the probabilities of the various configurations in each alignment for an initially randomly orientated disk around a given system.

1. INTRODUCTION

Circumbinary Observed circumbinary planets – those orbiting around two stars – have been mostly found to orbit in the same plane as their hosts (Doyle et al. 2011; Orosz et al. 2012; Welsh et al. 2012). However, Aly et al. (2015) and Martin & Lubow (2017) found that this is likely a result of selection effects (citations by David Martin..). Misaligned disks around eccentric binaries can evolve evolve either to coplanar (citations) to a polar state if their inclination is perturbed from coplanar (Aly et al. 2015; Martin & Lubow 2017). A polar-aligned debris disk has been found in the 99 Her system (Kennedy et al. 2012) and polar-aligned gas disks have been found in the HD 98800 (Kennedy et al. 2019) and V773 Tau systems (Kennedy et al. 2019; Kenworthy et al. 2022, respectively) (Kenworthy et al. 2022). AC Her, a post-AGB system with a polar-inclined disk, is believed to may host the first circumbinary planet found in a polar orbit (Martin et al. 2023) (??Martin et al. 2023).

The orbital parameters of these alignment of circumbinary planets, and the disks that they form from alignment of the disks from which they form, are determined from by their interaction history with their host stars. These interactions can be broadly For a massless circumbinary disk, the type of nodal precession can be split into two categories:

1. **Precession about the angular momentum vector of the binary.** In the case where the planet/disk is slightly misalignendmisalignend, its own angular momentum vector precesses about that of the binary (e.g., Bate et al. 2000; Lubow & Ogilvie 2000). This is characterized by near constant inclination and oscillation of the longitude of the ascending node. Included in this case is

the subclassification of retrograde orbits (those whose angular momentum vectors are misalignend by ~ 180 deg) and the two trivial cases of perfectly aligned/misalignend orbits which do not precess.

2. **Libration about the eccentricity vector of the binary.** In the case where misalignment is high (i.e. near perpendicular) the angular momentum vector of the planet/disk will librate precesses about the eccentricity vector of the binary (e.g., Verrier & Evans 2009; Farago & Laskar 2010; Doolin & Blundell 2011). This is called a librating orbit. In this case the mutual inclination of the disk oscillates about the polar configuration.

However, for a massive disk, there are additional types of nodal precession.... (describe) (Abod et al. 2022).

Planets form with the orbital characteristics given by their progenitor disks (e.g., Childs & Martin 2021), so it is sufficient in this work to discuss disk dynamics only. Differential precession between adjacent annular regions in a disk cause dissipation, ultimately dampening precession or libration so that the disk reaches a steady state on its viscous timescale (Bate et al. 2000, see also Nixon et al. (2011); Foucart & Lai (2013, 2014)). Therefore, it is appropriate to map a disk's initial interactions with a binary (prograde precession, libration, retrograde precession) to the disk's final configuration (prograde coplanar, circumpolar, retrograde coplanar, respectively).

In the case of a massless disk, the type of interaction can be determined analytically from just the binary eccentricity and the direction of the disk's specific angular momentum vector (parameterized by the disk inclination and its longitude of the ascending node Zanzazi &

Lai 2018). Given priors on these quantities we can predict the observed frequencies of circumbinary disks (and planets) in the polar configuration. Ceppi et al. (2024) do just this – finding the fractions of binaries with polar disks and the mean eccentricities of those binaries as a function of two free parameters.

In this work we will study the more general case of a massive disk. The resulting polar frequency function only contains one additional parameter, but the orbital parameters of the binary can now change due to interactions with the disk. The additional complications of this case require the application of numerical simulations; we use the N-body code **REBOUND** **rebound** (Rein & Liu 2012) to simulate the dynamics of a three-body system, with a massive point particle used as a stand-in for the disk. Abod et al. (2022) found that this 3-body setup is a valid description of a disk with angular momentum equal to that of the third body in the limit that the disk mass does not change (i.e. no accretion). This setup also cannot account for warping effects and disk breakage as we must treat the disk as a solid body. We describe this setup in detail in Section 2

[describe the regime we are working in]

2. METHODS

We describe two methods to approximate the evolution of a binary-disk system, each optimized for a different balance of computational cost and physical realism. First, we use the N-body code **REBOUND** **REBOUND** (Rein & Liu 2012) to simulate a 3-body system. The the disk using a point mass. The second method employs a Runge-Kutta-Fehlberg integrator to solve equations (7-10) from ?. These equations treat the central binary in the quadrupole approximation, but can be solved extremely efficiently. The code used to run these simulations is publically available¹.

2.1. *Simulation Setup* Geometric considerations

The dynamical state of the disk (i.e. prograde circulation, libration, etc.) is determined by tracking two relevant orbital elements: mutual inclination i and longitude of ascending node Ω . Each simulation method gives as an output the direction of the disk angular momentum relative to the binary \mathbf{l} . We define a coordinate system relative to the binary, with the z -axis to be along the angular momentum vector, the x -axis to be along the eccentricity vector, and the y -axis so that the coordinate system is right-handed.

The relevant coordinates are then defined

$$\cos i = \frac{\mathbf{l} \cdot \hat{\mathbf{z}}}{\|\mathbf{l}\|} \quad (1)$$

¹ https://github.com/tedjohnson12/misaligned_cb_disk

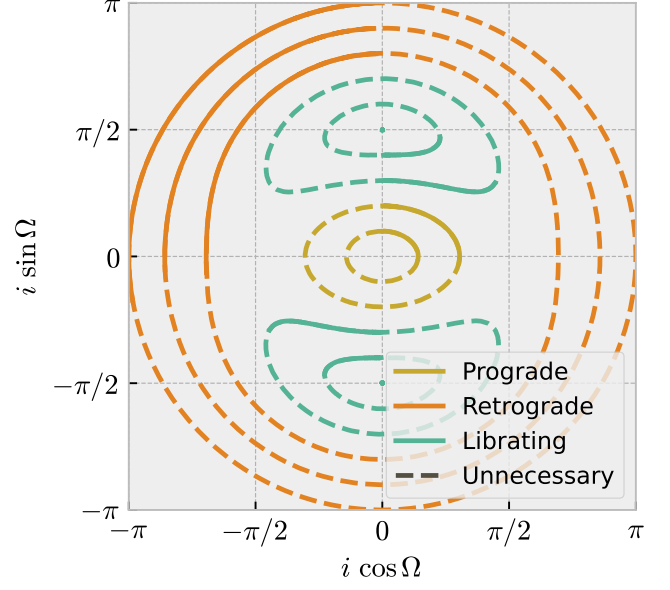


Figure 1. Example of system simulation and state determination. This figure tracks the orbital parameters of a massless third body orbiting a $1M_{\odot}$ binary with equal mass stars and $e_b = 0.4$. Initially $\Omega = \frac{\pi}{2}$. Solid lines indicate the portion of the simulation that is required to determine the state. Dashed lines complete the evolution back to the system’s initial conditions but are not needed for our analysis. In general, we will only integrate until the state of the system can be determined.

and

$$\Omega = \arctan2(\mathbf{l} \cdot \hat{\mathbf{x}}, -\mathbf{l} \cdot \hat{\mathbf{y}}) \quad (2)$$

Given some initial (i, Ω) , the system can be evolved forward in time to recover the familiar diagram shown in Figure 1. cite papers that have similar figures. This visualization also allows the dynamical state to be resolved programically, as a librating state will repeatedly cross the y -axis and never cross the x -axis, and a circulating state will sequentially cross each axis in an order that can determine if it is prograde or retrograde.

2.2. Using REBOUND

We use **REBOUND** **REBOUND**’s Python interface to initialize our simulation. Table 1 describes the simulation’s input parameters. We then integrate the system using the IAS15 15th order Gauss-Radau integrator (Rein & Spiegel 2015) until we can determine the system’s state.

2.2.1. *Determining the state*

We integrate the system 5 (third-body) orbits at a time, capturing the positions and velocities of each particle afterwards. Between each step we attempt to assign an end-state to the system. This is done by

name	symbol	type	description
mass_binary	M_b	float	The total mass of the binary in solar masses.
mass_fraction	f_b	float	The ratio between the secondary mass and the binary mass M_2/M_b .
semimajor_axis_binary	a_b	float	The semimajor axis of the binary orbit.
eccentricity_binary	e_b	float	The eccentricity of the binary orbit.
mass_planet	m_p	float	The mass of the third body.
semimajor_axis_planet	a_p	float	The semimajor of the third body orbiting the binary center of mass.
inclination_planet	i	float	The mutual inclination of the binary and the third body.
lon_ascending_node_planet	Ω	float	The longitude of the ascending node of the third body.
true_anomaly_planet	ν	float	The true anomaly of the third body.
gr	-	bool	Whether to include effects from general relativity.
eccentricity_planet	e_p	float	The eccentricity of the third body's orbit.
arg_pariapsis_planet	ω	float	The argument of periastron of the third body's orbit.

Table 1. REBOUND Simulation parameters

computing Not much can be learned from a single simulation as it only allows us to map from one point in (i, Ω) space to an end state. To infer the behavior of a population (and from that compute a polar fraction) we employ a Monte Carlo (MC) method, sampling isotropically on the (i, Ω) sphere. That is, $\Omega \in \mathcal{U}(0, 2\pi)$ and $i \in \{\arcsin(2u - 1) + \frac{\pi}{2} \mid u \in \mathcal{U}(0, 1)\}$.

Each MC run is initialized with the conditions of the binary as well as the angular momentum of the disk. We then sample i and Ω and checking them against two criteria:

1. Has $\Delta\Omega$ changed sign? In a precessing orbit Ω changes monotonically. If $\frac{d\Omega}{dt}$ changes from positive to negative (or vice-versa) then we can be sure we have found a librating state.
2. Has $i \sin \Omega$ crossed zero? In a librating state this quantity will never change sign.

Determining the state is done iteratively and only requires that i and Ω be known at each timestep. If neither criteria are true then we do not yet have enough information, and we continue the integration. If criterion ?? is true then the system is librating. If criterion ?? is true then the system is precessing. There is no know configuration that would allow both criteria to be true. in batches of four simulations, using a bootstrap metric after each batch to compute the polar fraction. Sampling stops when the bootstrap-computed confidence interval reaches a prescribed value. A typical simulation takes on the order of 0.1 – 1 s, so we save the results of each simulation in an SQLite database between batches. When an MC sampler is initialized it queries this database for all relevant passed simulations, ingests them, and only runs new simulations if a more stringent confidence interval is requested.

In order to compute i and Ω we must first define a coordinate system. REBOUND outputs the positions and velocities of each particle

in the center-of-mass frame. We then use the binary to define a time-dependent coordinate system. We define the z-axis to be along the angular momentum vector of

2.3. Runge-Kutta-Fehlburg method

In addition to using REBOUND in Section 2.2 we can solve the same problem using a slightly more analytical approach. ? found a set of first-order differential equations (their Equations 7-10) based on previous work by Farago & Laskar (2010) that describes the coupled behavior of the binary, the x-axis to be along the eccentricity vector, and the y-axis so that the coordinate system is right-handed disk angular momentum direction and the binary eccentricity. We solve these equations using the Runge-Kutta-Fehlberg (RKF) method ref? – a numerical method similar to the common 4th order Runge-Kutta integrator, but that computes a 5th order solution to allow for a variable step size. The cost of this method is that it treats the binary in the quadrupole approximation, meaning we are not sensitive to the effects of the binary mass fraction, but the computational cost is extremely low; we are able to run 10^4 - 10^5 simulations per second – about 10,000 times faster than REBOUND.

$$\begin{aligned}\hat{z} &= \vec{L} / \|\vec{L}\| \\ \hat{x} &= \vec{e} / \|\vec{e}\| \\ \hat{y} &= -\hat{x} \times \hat{z}\end{aligned}$$

We can then compute i and Ω from the specific angular momentum \vec{h} . The added computational efficiency means this method is not restricted to an MC method with hundreds of samples; we can compute a grid of $\sim 10^6$ in less than a minute to get a very accurate measure of the polar fraction.

$$\cos i = \frac{\vec{h} \cdot \hat{z}}{\|\vec{h}\|}$$

$$\Omega = \arctan2(\vec{h} \cdot \hat{x}, -\vec{h} \cdot \hat{y})$$

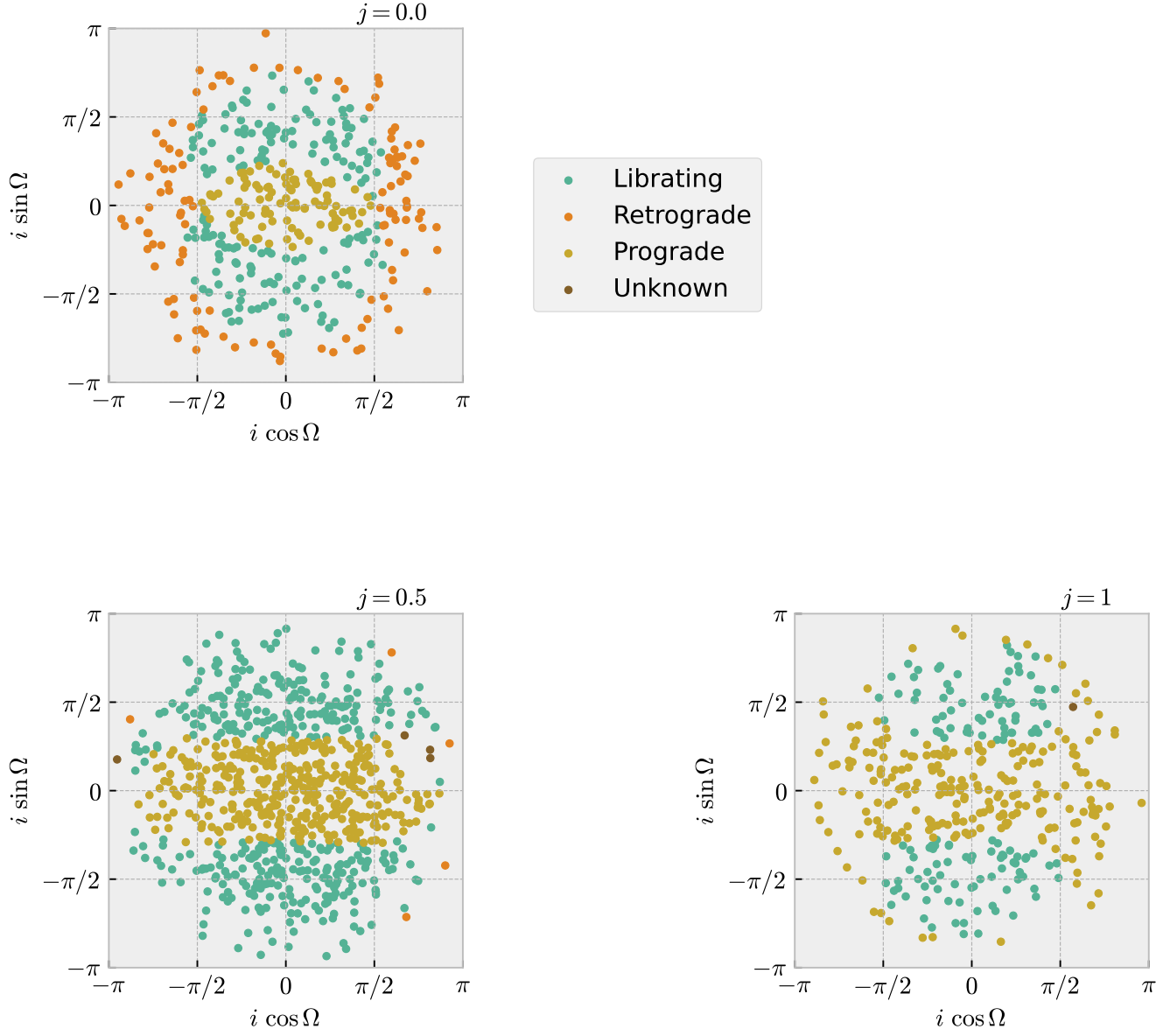


Figure 2. Monte Carlo results for a $1M_{\odot}$ equal mass binary with $e_b = 0.4$ for $j = 0, 0.5, 1$. The position of each point shows the initial condition of the simulation, and the color denotes the dynamical state. Note that some are marked as “unknown”. This is because we set a 1000 orbit limit on the integration for the sake of computational time.

Figure 1 shows a set of example simulations along with their determined states. Visualizing the system in this way makes it clear why we have chosen our two criteria. Librating orbits will never cross the x-axis and will cause the polar angle (Ω) to turn back before reaching 0 or π . Precessing orbits (both prograde and retrograde) travel approximately in circles with near-constant i .

3. RESULTS

4. DISCUSSION

5. CONCLUSIONS

6. ACKNOWLEDGEMENTS

This manuscript was prepared using the open-science software *show your work!* (Luger et al. 2021), making the article completely reproducible. The source code to

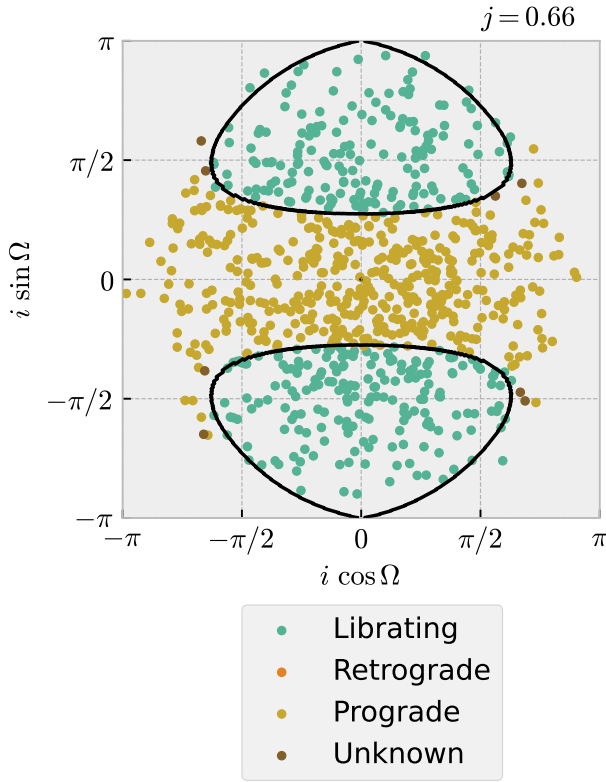


Figure 3. Example Contour lines denoting solution boundaries found via the RKF method compared to MC results of system simulation and state determination the same conditions. This figure tracks Binary setup is the orbital parameters of a massless third body orbiting a $1M_{\odot}$ binary with equal mass stars and $e_b = 0.4$ same as in Figure 2, but for $j = 0.66$, which is its critical value (see ?Abod et al. 2022). Initially $\Omega = \frac{\pi}{2}$. The grid here includes 250,000 points. Solid lines indicate the portion of the simulation that There is required some disagreement between RKF and REBOUND, which we attribute to determine misclassification due to behavior on the stateorbital timescale (i.e. small variations in Ω that cause the evolution back simulation to temporarily cross the system's initial conditions but are not needed for our analysis. In general y-axis twice, we will only integrate until giving the state false appearance of the system can be determined libration). We can fix this



compile this document and create the figures is available on GitHub².

Simulations in this paper made use of the REBOUND N-body code (Rein & Liu 2012). The simulations were integrated using IAS15, a 15th order Gauss-Radau integrator (Rein & Spiegel 2015).

Cherry Creek

REFERENCES

- Abod, C. P., Chen, C., Smallwood, J., et al. 2022, Monthly Notices of the Royal Astronomical Society, 517, 732, doi: 10.1093/mnras/stac2601
- Aly, H., Dehnen, W., Nixon, C., & King, A. 2015, Monthly Notices of the Royal Astronomical Society, 449, 65, doi: 10.1093/mnras/stv128
- Bate, M. R., Bonnell, I. A., Clarke, C. J., et al. 2000, Monthly Notices of the Royal Astronomical Society, 317, 773, doi: 10.1046/j.1365-8711.2000.03648.x

² <https://github.com/tedjohnson12/bin-disk-paper>

- Ceppi, S., Cuello, N., Lodato, G., et al. 2024, *Astronomy and Astrophysics*, 682, A104, doi: [10.1051/0004-6361/202348375](https://doi.org/10.1051/0004-6361/202348375)
- Childs, A. C., & Martin, R. G. 2021, *The Astrophysical Journal*, 920, L8, doi: [10.3847/2041-8213/ac2957](https://doi.org/10.3847/2041-8213/ac2957)
- Doolin, S., & Blundell, K. M. 2011, *Monthly Notices of the Royal Astronomical Society*, 418, 2656, doi: [10.1111/j.1365-2966.2011.19657.x](https://doi.org/10.1111/j.1365-2966.2011.19657.x)
- Doyle, L. R., Carter, J. A., Fabrycky, D. C., et al. 2011, *Science*, 333, 1602, doi: [10.1126/science.1210923](https://doi.org/10.1126/science.1210923)
- Farago, F., & Laskar, J. 2010, *Monthly Notices of the Royal Astronomical Society*, 401, 1189, doi: [10.1111/j.1365-2966.2009.15711.x](https://doi.org/10.1111/j.1365-2966.2009.15711.x)
- Foucart, F., & Lai, D. 2013, *The Astrophysical Journal*, 764, 106, doi: [10.1088/0004-637X/764/1/106](https://doi.org/10.1088/0004-637X/764/1/106)
- . 2014, *Monthly Notices of the Royal Astronomical Society*, 445, 1731, doi: [10.1093/mnras/stu1869](https://doi.org/10.1093/mnras/stu1869)
- Kennedy, G. M., Wyatt, M. C., Sibthorpe, B., et al. 2012, *Monthly Notices of the Royal Astronomical Society*, 421, 2264, doi: [10.1111/j.1365-2966.2012.20448.x](https://doi.org/10.1111/j.1365-2966.2012.20448.x)
- Kennedy, G. M., Matrà, L., Facchini, S., et al. 2019, *Nature Astronomy*, 3, 230, doi: [10.1038/s41550-018-0667-x](https://doi.org/10.1038/s41550-018-0667-x)
- Kenworthy, M. A., González Picos, D., Elizondo, E., et al. 2022, *Astronomy and Astrophysics*, 666, A61, doi: [10.1051/0004-6361/202243441](https://doi.org/10.1051/0004-6361/202243441)
- Lubow, S. H., & Ogilvie, G. I. 2000, *The Astrophysical Journal*, 538, 326, doi: [10.1086/309101](https://doi.org/10.1086/309101)
- Luger, R., Bedell, M., Foreman-Mackey, D., et al. 2021, *Mapping Stellar Surfaces III: An Efficient, Scalable, and Open-Source Doppler Imaging Model*, doi: [10.48550/arXiv.2110.06271](https://doi.org/10.48550/arXiv.2110.06271)
- Martin, R. G., & Lubow, S. H. 2017, *The Astrophysical Journal*, 835, L28, doi: [10.3847/2041-8213/835/2/L28](https://doi.org/10.3847/2041-8213/835/2/L28)
- Martin, R. G., Lubow, S. H., Vallet, D., Anugu, N., & Gies, D. R. 2023, *The Astrophysical Journal*, 957, L28, doi: [10.3847/2041-8213/ad0730](https://doi.org/10.3847/2041-8213/ad0730)
- Nixon, C. J., King, A. R., & Pringle, J. E. 2011, *Monthly Notices of the Royal Astronomical Society*, 417, L66, doi: [10.1111/j.1745-3933.2011.01121.x](https://doi.org/10.1111/j.1745-3933.2011.01121.x)
- Orosz, J. A., Welsh, W. F., Carter, J. A., et al. 2012, *The Astrophysical Journal*, 758, 87, doi: [10.1088/0004-637X/758/2/87](https://doi.org/10.1088/0004-637X/758/2/87)
- Rein, H., & Liu, S. F. 2012, *A&A*, 537, A128, doi: [10.1051/0004-6361/201118085](https://doi.org/10.1051/0004-6361/201118085)
- Rein, H., & Spiegel, D. S. 2015, *MNRAS*, 446, 1424, doi: [10.1093/mnras/stu2164](https://doi.org/10.1093/mnras/stu2164)
- Verrier, P. E., & Evans, N. W. 2009, *Monthly Notices of the Royal Astronomical Society*, 394, 1721, doi: [10.1111/j.1365-2966.2009.14446.x](https://doi.org/10.1111/j.1365-2966.2009.14446.x)
- Welsh, W. F., Orosz, J. A., Carter, J. A., et al. 2012, *Nature*, 481, 475, doi: [10.1038/nature10768](https://doi.org/10.1038/nature10768)
- Zanazzi, J. J., & Lai, D. 2018, *Monthly Notices of the Royal Astronomical Society*, 473, 603, doi: [10.1093/mnras/stx2375](https://doi.org/10.1093/mnras/stx2375)